Journal of the Optical Society of America B
OPTICAL PHYSICS

Nonlinear gas sensing based on third-harmonic generation in cascaded chalcogenide microfibers

Pan Huang,[1] Tianye Huang,[1,*] Shuwen Zeng,[2] Jianxing Pan,[1] Xu Wu,[1] Xiang Zhao,[1] Yiheng Wu,[1] Perry Shum Ping,[3] and Gilberto Brambilla[4]

[1]School of Mechanical Engineering and Electronic Information, China University of Geosciences (Wuhan), Wuhan 430074, China
[2]XLIM Research Institute, UMR 7252 CNRS/University of Limoges, 123, Avenue Albert Thomas, 87060 Limoges CEDEX, France
[3]Center of Fiber Technology, Electrical and Electronics Engineering, Nanyang Technological University, Singapore
[4]Optoelectronics Research Centre, University of Southampton, Southampton, Hampshire, UK
*Corresponding author: tianye_huang@163.com

Received 9 October 2018; revised 30 November 2018; accepted 12 December 2018; posted 13 December 2018 (Doc. ID 347835); published 16 January 2019

The performance of conventional gas sensors based on light absorption in the mid-infrared (MIR) faces the challenges of the high cost and low efficiency of photodetection at these wavelengths. In this paper, a nonlinear gas sensor based on third-harmonic generation (THG) in cascaded chalcogenide microfibers is proposed. In the first microfiber section, the input MIR light with "fingerprint" frequency has shown the ability for a large amount of gas absorption. The second microfiber section is used for THG pumped by the residual MIR light. In this process, the sensing signal is converted to the near-infrared region, and the power variation caused by the absorption is amplified due to the nonlinear relation between pump and harmonic signals. According to our analysis, the lowest methane concentration of 7.4×10^{-8} can be detected at a practically drawable Ae_2Se_3 microfiber length of 1 cm. Compared to direct MIR gas sensing, cascaded microfiber sensing has the advantages of improved sensing performance and also shorter absorption length.

https://doi.org/10.1364/JOSAB.36.000300

1. INTRODUCTION

Gas sensing plays a key role in environment monitoring and industrial inspection. The mid-infrared (MIR) spectrum (2.5–20 μm) is particularly attractive for this application, since a wide range of gases (including CO, CO_2, NO, NO_2, and CH_4) have telltale absorption fingerprints in this region, allowing quantitative, sensitive, and selective detection [1]. Most of the currently available remote sensors are based on optical detection that utilizes measurements of light absorption to determine the chemical composition of the sample. Tunable laser absorption spectroscopy (TLAS) has been demonstrated to have high sensitivity and good selectivity for real-time, *in situ* trace gas sensing [2,3]. And the development of a commercial room-temperature MIR laser has significantly boosted the sensitivity of a trace amount of gas detection. However, in MIR absorption spectroscopy, the laser signal is commonly monitored by a detector made of mercury cadmium telluride or indium antimonide, which have some drawbacks compared to silicon or gallium arsenide for the near-infrared (NIR) and visible wavelength ranges [4]. For example, due to the smaller energy band-gap, the MIR detector's sensitivity is significantly limited by thermal noise and must be cooled down constantly to obtain better performance [4]. Moreover, MIR detectors are not cost-effective for mass production. Compared to MIR detectors, the NIR counterparts can easily overcome these drawbacks. However, the gas absorption efficiency at this wavelength regime is much lower than MIR and consequently limits the overall sensing performance as well. For example, the absorption coefficient of methane at NIR is ~100 times lower than that of the one at MIR.

Nonlinear parametric upconversion is one of the most promising methods that can utilize not only the high absorption in MIR but also the high-performance photon detection in NIR [5–7]. In this scheme, the MIR light is first absorbed by the target gas with high efficiency. Then the residual MIR signal is converted to the NIR regime for detection through a nonlinear process. Therefore, the advantages of MIR absorption and NIR detection are fully obtained. Among the nonlinear effects for light upconversion, third-harmonic generation (THG) possesses the advantages of a large wavelength interval, a three-order exponential power scaling relation, and flexible platform choice, which makes it a potential approach for nonlinear gas absorption sensing.

Optical fiber has been demonstrated to be an effective medium for both gas sensing and THG [8–10]. However, it is well known that conventional silica fiber exhibited large propagation loss beyond 3 μm [11]. On the contrary, soft glasses possess excellent optical transparency in MIR.

Particularly, chalcogenide glass shows broad transmission range from 1 to 16 μm, and its high nonlinear refractive index up to a magnitude of 10^{-17} m^2/W is suitable and favorable for both sensing and nonlinear optics [12]. Because of such high nonlinearity and strong evanescent field, chalcogenide microfibers show great potential in nonlinear gas sensing. To date, the chalcogenide microfibers have usually been cladded or coated by polymers to improve their physical strength in the tapering process [13,14]. Nonetheless, the polymer cladding can induce high absorption in the MIR region [15,16]. Fortunately, a direct chalcogenide fiber tapering method can also be used to draw a uniform As_2Se_3 microfiber [15], which provides more practical operability for microfiber sensors in the MIR regime.

In this paper, a nonlinear gas sensor based on THG in cascaded chalcogenide microfibers is demonstrated for detecting methane as the target molecule, which is a strong greenhouse gas and the main component of life energy. In the first section of the cascaded microfiber, the MIR fingerprint light is absorbed by the target gas through evanescent field interaction, while the second one is designed to meet the phase matching condition (PMC) for THG. In this way, the harmonic radiation at NIR is produced by the residual MIR light. The detection limit (DL) is studied by analyzing the fiber structure and also comparing it with the one based on direct MIR absorption. It is shown that the cascade microfiber sensor has great advantages over MIR sensing in terms of detection sensitivity and absorption length at ultra-low gas concentrations.

2. STRUCTURE AND THEORY

A. Gas Sensor Design

The schematic of the gas sensor based on cascaded microfiber is shown in Fig. 1. Two sections of microfibers are cascaded for MIR gas absorption and THG, respectively. As_2Se_3 glass, which owns a nonlinear refractive index of 2.4×10^{-17} m^2/W [12], is selected as the single material for the microfiber design. The shadow region represents a mixed gas chamber containing methane with a strong absorption peak at 3300 nm wavelength with an absorption coefficient of 1.6/cm [13]. The lengths of the first section for gas absorption and the second section for THG are L_1 and L_2, respectively.

The diameters of the two sections of microfibers are determined by the evanescent field and PMC, which promise efficient absorption and nonlinear conversion, respectively. For THG, assuming that self-phase modulation and cross-phase modulation corrections to the propagation constants are small, the PMC is roughly equivalent to the effective index of the fundamental wave (FW), which is equal to one third-harmonic wave (THW) [17]. Figure 2(a) shows the dispersion relations between the fundamental mode $HE_{11}(\omega)$ of the FW

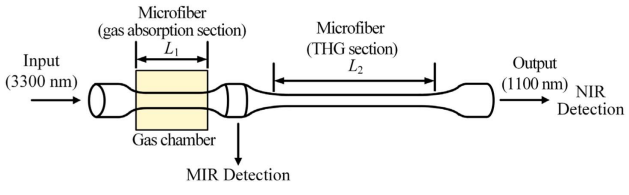

Fig. 1. Schematic of gas sensing based on cascaded microfiber.

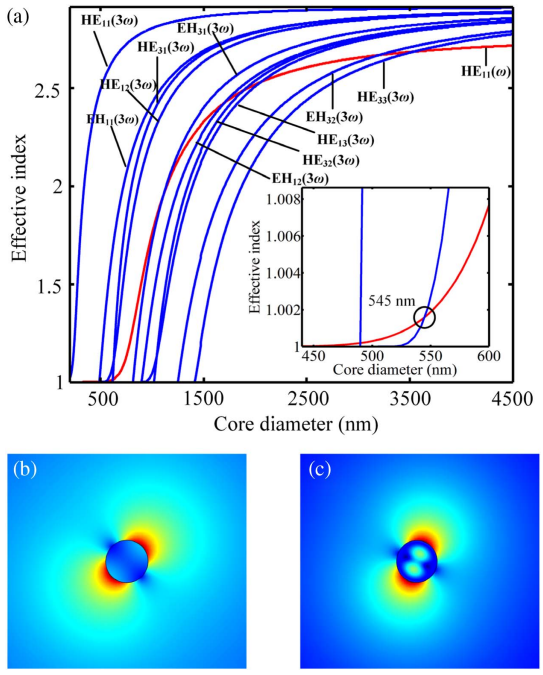

Fig. 2. (a) Dispersion relation of the fundamental mode (HE_{11}) of FW ($\lambda_1 = 3300$ nm, red) and the HOMs of the THW ($\lambda_3 = 1100$ nm, blue). ω is the frequency of the FW, and 3ω is the frequency of the THW. For the PMC for wave vectors of the FW and THW, we have the propagation constant mismatch $\delta\beta = \beta_3 - 3\beta_1 = n_{\text{eff}}(3\omega) \cdot 2\pi/\lambda_3 - 3n_{\text{eff}}(\omega) \cdot 2\pi/\lambda_1 = 0$, which is equivalent to $n_{\text{eff}}(3\omega) = n_{\text{eff}}(\omega)$. (b),(c) Optical field distribution corresponding to (b) HE_{11} mode of FW and (c) HE_{12} mode of THW.

($\lambda_1 = 3300$ nm) and the high-order modes (HOMs) of the THW ($\lambda_3 = 1100$ nm) for As_2Se_3 microfiber. Ideally, the fundamental modes of both waves should be the best choice for PMC. However, it is difficult to achieve such a condition because of the existence of material dispersion. On the contrary, plenty of HOMs satisfy the PMC. Nevertheless, they have different mode overlap with the FW. Here we choose mode $HE_{12}(3\omega)$, which offers the best mode overlap for THG with the fiber diameter of 545 nm. And as seen from Figs. 2(b) and 2(c), the optical field distributions of HE_{11} of FW and HE_{12} of THW have a high degree of coincidence. Different from the second fiber section, the first one is expected for pure gas absorption without THG, and therefore PMC should be avoided. Furthermore, for high-efficiency absorption, a large evanescent field is preferred. The evanescent field can be characterized by the confinement factor, which indicates the overlap between the gas and the mode field:

$$\Gamma = \frac{\iint \boldsymbol{S}_{\text{claddingz}} \mathrm{d}x\mathrm{d}y}{\iint \boldsymbol{S}_{\text{totalz}} \mathrm{d}x\mathrm{d}y}, \tag{1}$$

where $\boldsymbol{S}_{\text{claddingz}}$ and $\boldsymbol{S}_{\text{totalz}}$ represent the longitudinal component of the Poynting vector of the environmental cladding and the total microfiber, respectively.

For 3300 nm wavelength, the confinement factor corresponding to different microfiber diameters is shown in Fig. 3. The confinement factor decreases as the core diameter

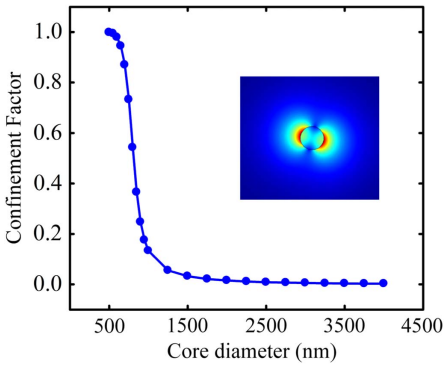

Fig. 3. Confinement factor corresponding to different core diameters of As_2Se_3 microfiber with the incident wavelength of 3300 nm. (Inset: optical field distribution corresponding to the core diameter of 750 nm.)

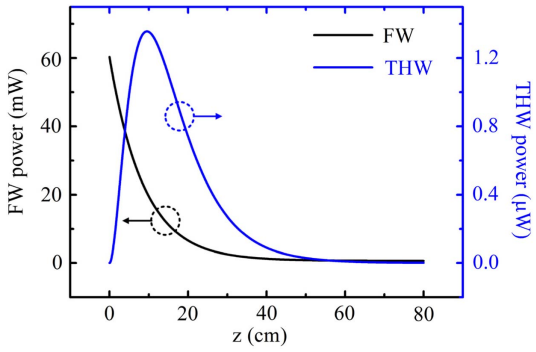

Fig. 4. Power evolution of FW ($\lambda_1 = 3300$ nm, black line) and THW ($\lambda_3 = 1100$ nm, blue line) in THG. Hereon, $L_1 = 5$ cm, $L_2 = 10$ cm, $C = 1 \times 10^{-8}$, and $P_0 = 0.1$ W.

increases, which shows a sharp decline from core diameter of 0.5 μm to 1 μm. And then when the core diameter sequentially increases, the confinement factor tends to be negligible. This phenomenon is due to the more tightly confined the optical mode field in the core with diameter increment. Taking these into consideration, in order to enhance the light–gas interaction and induce large phase mismatch, the core diameter of the first section is determined to be 750 nm with the confinement factor of 0.733. The inset picture in Fig. 3 shows the strong evanescent field of the As_2Se_3 microfiber with a core diameter of 750 nm.

B. Theoretical Model

For methane sensing, light at the methane "fingerprint" wavelength of 3300 nm is launched into the chalcogenide fiber and then propagates along the first microfiber section, which is assumed to immerse in a closed mixed gas chamber. According to the Beer–Lambert Law, the output power P_1 of the first-section microfiber after gas absorption can be defined [18]:

$$P_1 = P_0 \exp(-\sigma C \Gamma L_1 - \alpha L_1), \tag{2}$$

where P_0 is the input power, σ (1.6/cm for methane) is the absorption coefficient of 100% gas, C is the volume concentration of methane, $\alpha = \alpha_{\mathrm{dB}}/4.343$ is attenuation coefficient, and Γ is the confinement factor.

For THG, it can be modeled by the following coupled-mode equations [17]:

$$\begin{aligned}\frac{\partial A_1}{\partial z} &= i n_2 k_1[(J_1|A_1|^2 + 2J_2|A_3|^2)A_1 + J_3 A_1^{*2} A_3 \\ &\quad \times \exp(i\delta\beta z)] - \frac{\alpha_1}{2}A_1, \\ \frac{\partial A_3}{\partial z} &= i n_2 k_1[(6J_2|A_1|^2 + 3J_5|A_3|^2)A_3 + J_3^* A_1^3 A_3 \\ &\quad \times \exp(i\delta\beta z)] - \frac{\alpha_3}{2}A_3,\end{aligned} \tag{3}$$

where A_1 and A_3 are the amplitudes of the modes corresponding to FW and THW, respectively, z is the propagation distance, $\alpha_1 = \alpha_{\mathrm{dB}}/4.343$ and $\alpha_3 = \alpha_{\mathrm{dB}}/4.343$ [α_{dB} is the intrinsic loss, and the factor 4.343 is the conversion factor from loss (dB/m) to attenuation coefficient (/m)] are the attenuation coefficients of FW and THW, respectively, $\delta\beta = \beta_3 - 3\beta_1$ is the propagation constant mismatch, $k_1 = \omega_1/c = 2\pi/\lambda_1$ is the propagation constant of FW in vacuum, n_2 is the nonlinear refractive index coefficient of fiber material, and J_i are nonlinear overlap integrals. For $\mathrm{HE}_{11}(\omega)$ and $\mathrm{HE}_{12}(3\omega)$ modes, $J_1 = 0.053\ \mu\mathrm{m}^{-2}$, $J_2 = 0.073\ \mu\mathrm{m}^{-2}$, $J_3 = 0.057\ \mu\mathrm{m}^{-2}$, and $J_5 = 0.011\ \mu\mathrm{m}^{-2}$.

The output power of the first section is the pump power for THG in the second section. As the light propagates in the second-section fiber, the energy of FW is gradually converted to THW. It can be seen from Fig. 4 that with a 0.1 W pump, the power of THW increases to a maximum value and then decreases gradually to 0. The maximum THG power is 1.34 μW, which can be easily detected by the commercially available NIR detectors.

The DL can be defined as the minimum concentration that can be measured (C_{min}) by the sensor, which is determined by the resolution of the detector (P_{min}) [19]. Here, P_{min} can be represented by the difference between the output power $P(C = 0)$ for a zero concentration and the output power $P(C = C_{\mathrm{min}})$ for the minimum concentration:

$$P_{\mathrm{min}} = P(C = 0) - P(C = C_{\mathrm{min}}). \tag{4}$$

In practice, P_{min} is dominated by the performance of the photodetector. In our analysis, the power detection resolution of 1×10^{-9} W for MIR detection and the one of 1×10^{-13} W for NIR detection were assumed [1]. The sensitivity S is defined as the differential of output power variation to the gas concentration:

$$S = \left|\frac{dP}{dC}\right|, \tag{5}$$

where $P = P(C)/P(C = 0)$ is the normalized power. The benefit of using normalized power is that the relative value of the output power provides comparability for the sensitivity between MIR detection and NIR detection as shown in Fig. 1.

As the generated THW power is small ($|A_3| \ll |A_1|$), the approximate solution of Eq. (3) can be expressed as [17]

$$P_3 \approx P_1^3 (k_1 n_2 |J_3|)^2 z^2, \tag{6}$$

where P_3 is the power of the THW. And hence the sensitivity related to normalized power of MIR detection and NIR

detection in the cascaded microfiber sensor can be calculated, respectively, as

$$S_{\mathrm{MIR}} = \delta\Gamma L_1 \exp(-\delta\Gamma C L_1), \tag{7}$$

$$S_{\mathrm{NIR}} = 3\delta\Gamma L_1 \exp(-3\delta\Gamma C L_1). \tag{8}$$

Thus, considering the trace gas concentrations, for the same C and L_1, the sensitivity of NIR detection is ~3 times that of MIR detection.

3. RESULTS AND DISCUSSION

In this section, the performance of the designed cascaded chalcogenide microfiber gas sensor is studied. As can be seen from Fig. 1, the output power of the two sections of microfibers is recorded by the MIR detector and the NIR detector, respectively. Considering the fiber damage threshold, the input power is fixed at 0.1 W. Furthermore, in order to simplify the analysis, the intrinsic loss of $\alpha_{\mathrm{dB}} = 0.5$ dB/cm for both 3300 and 1100 nm wavelengths is considered here.

A. Ideal Interaction Lengths for the Cascaded Microfiber Sensor

As shown in Fig. 5, the power evolution of the THW in the second-section microfiber with different L_1 was studied. As L_1 increases, the achievable power of the THW decreases for the same L_2 due to higher absorption. The four curves have the same characteristics with maximum THW power at $L_2 = \sim 9.5$ cm. The microfiber length corresponding to the minimum DL can be considered as the optimal length (L_{opt}). Therefore, L_{opt} of the THG section for the designed cascaded chalcogenide microfiber sensor is 9.5 cm.

After determining the optimum length for THG, the DL of the cascaded microfiber sensing at different L_1 was calculated. In order to make a comparison with direct MIR sensing, the DL of direct MIR sensing was also calculated. As shown in Fig. 6, with L_1 increment, DL decreases first and then increases for both direct MIR detection and NIR detection, which indicates the existence of the optimum L_1. The minimum DLs for these two sensing schemes are 2.7×10^{-9} and 3.50×10^{-9}, respectively. Correspondingly, the L_{opt} of the gas absorption section for direct MIR sensing is ~8.7 cm, while L_{opt} of the absorption section for cascaded microfiber sensing is ~2.9 cm, which is 1/3 of the one for direct MIR sensing. Therefore, the DL of the upconversion detection sensing scheme is comparable with the direct MIR one but with much shorter absorption length. Such shorter light–gas interaction length is essential to mitigate the influence of the concentration gradient.

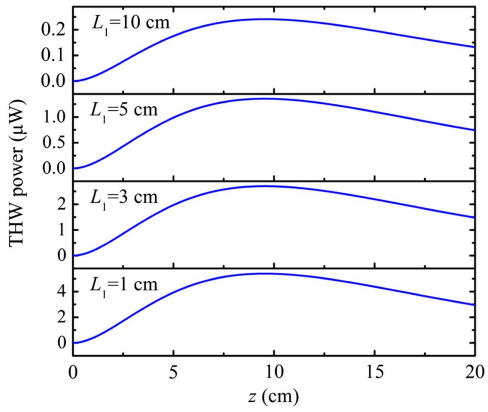

Fig. 5. Power evolution of THW with propagation distance increment in the second section of microfiber at $L_1 = 1$ cm, 3 cm, 5 cm, and 10 cm, respectively. Hereon, $C = 1 \times 10^{-8}$ and $P_0 = 0.1$ W.

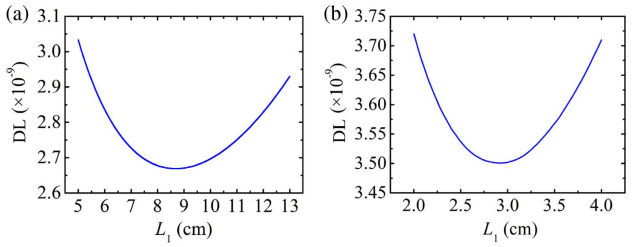

Fig. 6. DL for (a) MIR sensing and (b) cascaded microfiber sensing at different L_1. Hereon, $L_2 = 9.5$ cm and $P_0 = 0.1$ W.

Figure 7 shows the sensitivity and normalized power corresponding to different gas concentrations C for MIR detection and NIR detection under optimal lengths $L_1 = 2.9$ cm and $L_2 = 9.5$. With C increment, the normalized output power of both MIR detection and NIR detection decreases, but the variation of THW power is more drastic at low concentrations, resulting in higher sensitivity, as shown in Fig. 7(b). More importantly, the NIR detection scheme has higher sensitivity when the target gas concentration is less than ~0.16. When C is close to 0, the sensitivity of NIR detection is ~3 times that of MIR detection, which matches well with the theoretical analysis. Therefore, the proposed cascaded chalcogenide microfiber sensor is more suitable for low concentration detection.

In order to investigate the effect of the gas absorption length on the critical concentration (the concentration when the sensitivity of MIR detection and NIR detection is equal), the critical concentrations at different L_1 are given in Fig. 8. As L_2 has a negligible effect on the sensitivity according to Eq. (5), L_2 is fixed with 9.5 cm. The critical concentration decreases and tends to be 0 as L_1 increases, which means that when the gas absorption length is large enough, the advantage of the cascaded microfiber sensing in detection sensitivity fades away. However, the length of a microfiber is limited by the fabrication

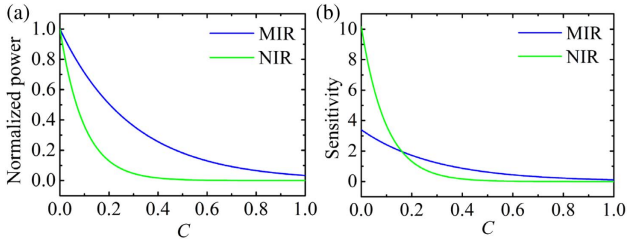

Fig. 7. (a) Normalized output power of the first-section microfiber (MIR detection, blue line) and the second-section microfiber (NIR detection, green line). (b) Sensitivity of MIR detection (blue line) and NIR detection (green line) in the cascaded microfiber sensor. Hereon, $P_0 = 0.1$ W, $L_1 = 2.9$ cm, and $L_2 = 9.5$ cm.

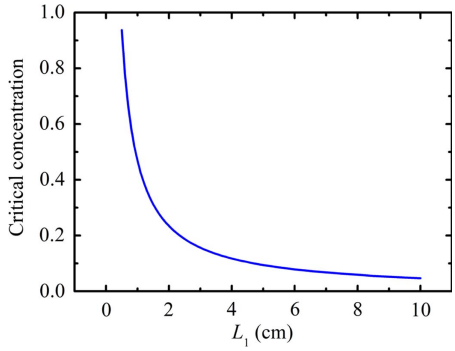

Fig. 8. Critical concentrations at different L_1.

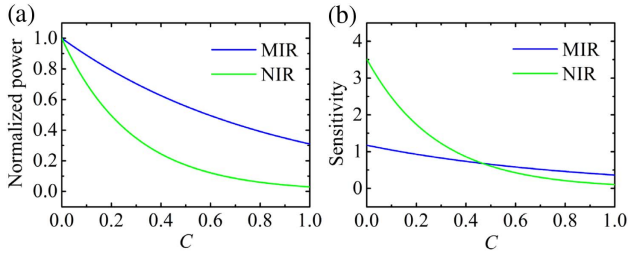

Fig. 9. (a) Normalized output power of the first-section microfiber (MIR detection, blue line) and the second-section microfiber (NIR detection, green line). (b) Sensitivity of MIR detection (blue line) and NIR detection (green line) in the cascaded microfiber sensor. Hereon, $P0 = 0.1$ W, $L_1 = 1$ cm, and $L_2 = 1$ cm.

techniques. Hence, the proposed sensing scheme can be used to reduce the absorption length.

B. Practical Interaction Lengths for the Cascaded Microfiber Sensor

It should be noted that fabricating uniform microfiber with length of several centimeters is still challenging. In practice, to the best of our knowledge, a pure As_2Se_3 fiber now can be tapered up to a maximum length of ~1 cm with a diameter of below 1 μm [15]. Therefore, it is necessary to take this into consideration.

It can be seen from Fig. 9 that the cascaded microfiber sensor with $L_1 = 1$ cm and $L_2 = 1$ cm still exhibits better sensitivity at concentrations below ~0.48, which matches well with the critical concentration at $L_1 = 1$ cm in Fig. 8. Furthermore, the DL of NIR detection is 7.4×10^{-8}, which is better than the 9.6×10^{-8} obtained by direct MIR detection.

4. CONCLUSION

In summary, a nonlinear gas sensor based on THG in cascaded chalcogenide microfibers is proposed. Two sections of microfibers are used for MIR "fingerprint" spectrum absorption and THG-based MIR-to-NIR upconversion, respectively. Compared to the direct MIR sensing scheme, the proposed cascaded microfiber sensor provides the advantages of shorter MIR absorption length and higher sensitivity at low gas concentrations. By optimizing the parameters, the proposed cascaded chalcogenide microfiber sensor can detect the target methane concentration to a limit as low as 3.5×10^{-9} theoretically. Under the practical condition of $L_1 = L_2 = 1$ cm, the cascaded microfiber sensor can detect the minimum methane concentration of 7.4×10^{-8}, which is significantly improved by 30% in comparison to that of direct MIR sensing with the same gas absorption length. In addition, besides methane, this sensing scheme can be easily extended for other gases.

Funding. National Natural Science Foundation of China (NSFC) (61605179); Wuhan Science and Technology Bureau (2018010401011297); The Fundamental Research Funds for the Central Universities, China University of Geosciences, Wuhan (CUG) (162301132703, CUG2018JM16, G1323511794); The Experimental Technology Research Funds (SJ-201816).

REFERENCES

1. A. Gutierrez-Arroyo, E. Baudet, L. Bodiou, V. Nazabal, E. Rinnert, K. Michel, B. Bureau, F. Colas, and J. Charrier, "Theoretical study of an evanescent optical integrated sensor for multipurpose detection of gases and liquids in the mid-infrared," Sens. Actuators B Chem. **242**, 842–848 (2017).
2. M. W. Sigrist, R. Bartlome, D. Marinov, J. M. Rey, D. E. Vogler, and H. Wätcher, "Trace gas monitoring with infrared laser-based detection schemes," Appl. Phys. B **90**, 289–300 (2008).
3. L. Liu, B. Xiong, Y. Yan, J. Y. Li, and Z. H. Du, "Hollow waveguide-enhanced mid-infrared sensor for real-time exhaled methane detection," IEEE Photon. Technol. Lett. **28**, 1613–1616 (2016).
4. S. Wolf, T. Trendle, J. Kiessling, J. Herbst, K. Buse, and F. Kühnemann, "Self-gated mid-infrared short pulse upconversion detection for gas sensing," Opt. Express **25**, 24459–24468 (2017).
5. L. Høgstedt, J. S. Dam, A. Sahlberg, Z. S. Li, M. Aldén, C. Pedersen, and P. Tidemand-Lichtenberg, "Low-noise mid-IR upconversion detector for improved IR-degenerate four-wave mixing gas sensing," Opt. Lett. **39**, 5321–5324 (2014).
6. A. Barh, P. Tidemand-Lichtenberg, and C. Pedersen, "Thermal noise in mid-infrared broadband upconversion detectors," Opt. Express **26**, 3249–3259 (2018).
7. G. S. Maciel, L. de S. Menezes, A. S. L. Gomes, C. B. de Araújo, Y. Messaddep, A. Florez, and M. A. Aegerter, "Temperature sensor based on frequency upconversion in Er^{3+}-doped fluoroindate glass," IEEE Photon. Technol. Lett. **7**, 1474–1476 (1995).
8. K. H. Lee, W. Y. Choi, Y. A. Leem, K. S. Choi, H. Ko, and K. H. Park, "Harmonic signal generation and frequency up-conversion using a hybrid mode-locked multisection DFB laser," IEEE Photon. Technol. Lett. **19**, 901–903 (2007).
9. M. Hikita, Y. Hiraizumi, H. Aoki, J. Matsuda, and T. Watanade, "Experiments for self-temperature compensated characteristics of SAW gas sensor at fundamental and third-harmonic frequencies," Electron. Lett. **45**, 1101–1102 (2009).
10. D. Kartashov, S. Ališauskas, A. Pugžlys, A. A. Voronin, A. M. Zheltikov, and A. Baltuška, "Third- and fifth-harmonic generation by mid-infrared ultrashort pulses: beyond the fifth-order nonlinearity," Opt. Lett. **37**, 2268–2270 (2012).
11. T. Izawa, N. Shibata, and A. Takeda, "Optical attenuation in pure and doped fused silica in the IR wavelength region," Appl. Phys. Lett. **31**, 33–35 (1977).
12. B. Ung and M. Skorobogatiy, "Chalcogenide microporous fibers for linear and nonlinear applications in the mid-infrared," Opt. Express **18**, 8647–8659 (2010).
13. R. Ahmad, M. Rochette, and C. Baker, "Fabrication of Bragg gratings in subwavelength diameter As_2Se_3 chalcogenide wires," Opt. Lett. **36**, 2886–2888 (2011).

14. L. Z. Li, A. Al-Kadry, N. Abdukerim, and M. Rochette, "Design, fabrication and characterization of PC, COP and PMMA-cladded As_2Se_3 microwires," Opt. Mater. Express **6**, 912–921 (2016).
15. O. Aktas and M. Bayindir, "Tapered nanoscale chalcogenide fibers directly drawn from bulk glasses as optical couplers for high-index resonators," Appl. Opt. **56**, 385–390 (2017).
16. S. Shabahang, G. Tao, J. J. Kaufman, and A. F. Abouraddy, "Dispersion characterization of chalcogenide bulk glass, composite fibers, and robust nanotapers," J. Opt. Soc. Am. B. **30**, 2498–2506 (2013).
17. V. Grubsky, "Glass micro-fibers for efficient third harmonic generation," Opt. Express **13**, 6798–6806 (2005).
18. Z. Han, P. Lin, V. Singh, L. Kimerling, J. Hu, K. Richardson, A. Agarwal, and D. T. H. Tan, "On-chip mid-infrared gas detection using chalcogenide glass waveguide," Appl. Phys. Lett. **108**, 141106 (2016).
19. J. Charrier, M. L. Brandily, H. Lhermite, K. Michel, B. Bureau, F. Verger, and V. Nazabal, "Evanescent wave optical micro-sensor based on chalcogenide glass," Sens. Actuators B Chem. **173**, 468–476 (2012).